Silicon Carbide Oscillators for Extreme Environments

D.R. Brennan, H.K. Chan, N.G. Wright

School of Engineering, Newcastle University, Newcastle NE1 7RU, UK

A.B. Horsfall

Department of Engineering, University of Durham, Durham, DH1 3LE, UK

Introduction

Silicon carbide based electronics have the advantage of being highly radiation resistant and capable of operating at temperatures not possible with conventional, silicon based technologies [1]. This allows for their utilisation as sensor circuits for applications located in hazardous environments, which are often inaccessible or hazardous to personnel. For this reason, it is desirable for the circuit to include some form of wireless communication capability that is realised with silicon carbide based components. In electronics there is a standard requirement for repetitive waveforms to perform multiple functions, including the carrier waves required for communications systems. In order to meet this requirement, oscillator circuits are required, which depending on complexity can produce any waveform including high frequency radio waves. These high frequency radio signals form the basis of wireless communication systems. The challenge in realising these high frequency oscillators for deployment in these extreme environments is the lack of process maturity in silicon carbide and the shift in the performance with temperature. This chapter provides an overview of a range of oscillator circuit topologies that are compatible with analog circuits designs and hence existing silicon carbide technology, before on focusing on the realisation of a high temperature Colpitts Oscillator, which is used to demonstrate a high temperature prototype communication circuit. The drift of the central frequency with temperature of Silicon Carbide based oscillators is reported and described in terms of the parametric characteristics of the devices. The circuit is then expanded to enable the first silicon carbide Colpitts oscillator based Voltage Controlled Oscillator (VCO), which is presented as a method of enabling the closed loop control of the frequency of an oscillator over a wide temperature range. The chapter concludes with demonstrations of both Amplitude and Frequency Modulation of carrier waves from a circuit operating at 300 °C and subsequently discussed with a view to creating a high temperature wireless communication system.

Silicon carbide technology overview

The development of silicon carbide (SiC) technology has become increasingly rapid in recent years. With the significant improvements in wafer growth technology and materials processing, SiC devices have become part of the mainstream in power electronic applications [2,3] and a number of conferences are running dedicated sessions to the deployment of this technology in mainstream applications. Further advantages in terms of small, signal level devices [4] and sensors [5] have resulted in significant improvements in capabilities, however these are still only available at research level, where a number of groups are active. The underlying rationale for the continued investment in SiC technology is the excellent material properties, which derive from the high chemical stability of the Si-C bond. SiC is the only technologically relevant semiconductor that has a stable thermal oxide (SiO_2) [6] and can exist in a large number of polytypes – different crystal structures built from the same Si-C sub-unit organised into different stacking sequences. There are over 100 of these polytypes known, however, the vast majority of the research has focussed on three: 3C, 6H and 4H. Of these, the 4H polytype is the most common for electronic devices and the commercially available power electronic devices are manufactured almost exclusively from this polytype, due to its overall superior material properties. The bandgap of 4H SiC is 3.23eV at room temperature (compared to 1.12eV for silicon) and this dramatically reduces the intrinsic carrier concentration in comparison to semiconductors such as silicon or gallium arsenide and this allows devices to theoretically operate at temperatures up to 1000 °C [7]. SiC also has a high saturation electron velocity, $2 \times 10^7 \mathrm{cm \cdot s^{-1}}$, a thermal conductivity in excess of copper at room temperature and a critical electric field that is almost an order of magnitude higher than that of silicon. These parameters have been exploited in the high performance power MOSFETs and diodes that are commercially available, but also have the potential to realise high performance, high frequency oscillators.

The electronic oscillator

An electronic oscillator is a circuit which produces a repetitive, oscillating signal; converting a direct current (DC) power supply in to an alternating current (AC) signal. The shape of the required signal waveform depends on the application for which the oscillator is designed and typical examples include the generation of clock pulses for digital electronics [8], pulse width modulated switching waveforms for switch mode power supplies [9], and radio frequency signals for wireless electronic communications [10]. A significant number of oscillator circuits have been realised, however they can be categorised as two main types: the nonlinear oscillator and the linear or harmonic oscillator.

The non–linear oscillator

The nonlinear oscillation (sometimes referred to as a relaxation oscillator) produces a waveform that is non sinusoidal, such as a square wave, sawtooth or triangular waveform. The circuit topology comprises an energy storage component in conjunction with a nonlinear switching circuit. The energy storage component is often a capacitor, however circuits based on the use of inductors have been demonstrated. Alternative implementations of this circuit include those that include a negative resistance device, that periodically charges and discharges the energy in the storage element, resulting in abrupt changes in the output voltage of the circuit. Square wave relaxation oscillators are used extensively in digital electronics to provide the clock signal for sequential logic circuits such as timers and counters, whereas sawtooth oscillators are used specifically in time base circuits. An example of a single active device relaxation oscillator can be constructed using a device Uni-Junction Transistor (UJT). A UJT comprises of one P-N junction, making it similar in structure to a p-n diode, however it differs in the fact that it has three terminals and so is also referred to as a double base diode. It is worth noting that whilst the UJT has a similar construction to a Junction Field Effect Transistor (JFET), the operation in a circuit is significantly different. In a UJT the current through the device is modulated by the bipolar current injected through the gate under forward bias, rather than by the influence of the depletion region formed in the channel [11] with the gate under reverse bias.

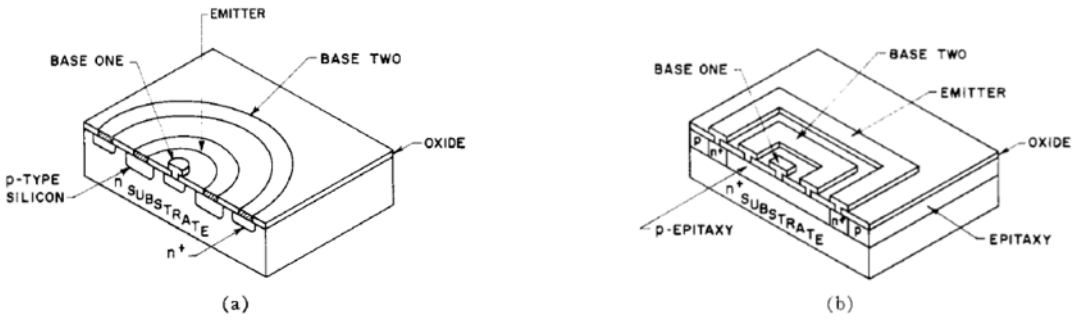

Figure 1: Example of the physical construction of a UJT (a) Diffused planar structure and (b) Epitaxial planar structure [12]

As can be seen from figure 1 the structure of a UJT does show some similarity to that of an N-channel JFET. The device consists of a lightly doped n type substrate with three p-type terminals, which are labelled as Base one (B_1), Base two (B_2) and an Emitter (E). B_1 and B_2 are ohmic contacts formed on the n^- epilayer, whereas the E is formed from a heavily doped p–type region. The main physical difference between the UJT and a JFET is that p–type region completely surrounds the n–type region in a JFET and the surface area of the JFET gate is significantly larger than area of the emitter junction in the UJT. In a typical UJT, the doping of the emitter region is high, whilst the dopant concentration in the n– type region is low. This results in the resistance between the

base terminals being significantly higher than is typical for a JFET, being in the region of 4 to 10 kΩ when the emitter is open circuit. In practical devices, the n–type channel has a high resistance and the resistance between the emitter and contact B_1 is larger than that between the emitter and B_2, resulting from the physical asymmetry in the structure i.e. the emitter is physically closer to B_2 than B_1

A UJT does not have the ability to amplify, however is capable of controlling a large ac power with a small signal applied to the gate. In operation the UJT is biased with a positive voltage between the two bases, whereby B_2 is biased more positively than B_1, resulting in a potential drop to be created along the length of the device. This can be seen in the schematic representation of a UJT shown in figure 2a. When the emitter voltage is greater than the voltage applied to B_2 plus the built–in potential of the p-n junction (typically 0.7 V for silicon and 2.8 V for SiC [13]), current flows from the emitter into the base region. Because the base region is very lightly doped, the additional charge carriers in the base region, that are injected by the emitter current, resulting in conductivity modulation. This excess charge reduces the resistance of the base region between the emitter junction and the B_2 contact. This reduction in resistance results in the potential difference between the emitter and B_1 increasing, which means that the emitter junction is more forward biased, and so even more current is injected. Overall, the effect appears to be similar to a negative resistance at the emitter terminal. This apparent negative resistance is the property that makes the UJT useful as the active component in simple oscillator circuits.

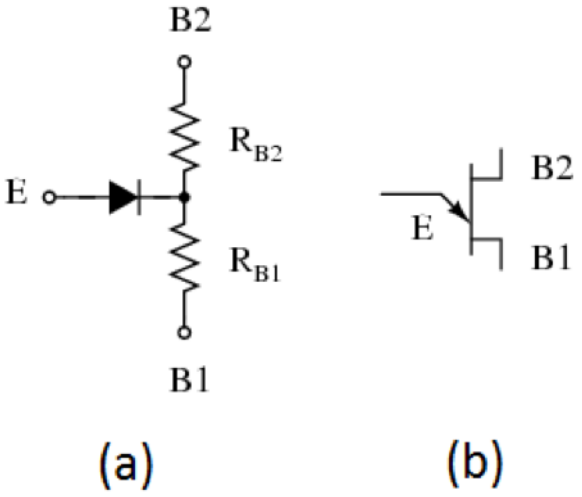

Figure 2: (a) Schematic representation of a UJT (b) Circuit symbol of a UJT

With the emitter open circuit, it is possible to determine the total resistance of the channel also known as interbase resistance $R_{BB0)}$ as:

$$R_{BB0} = R_{B_1} + R_{B_2} \tag{1}$$

As described previously, practical devices are non symmetrical and therefore it is possible to express the ratio between the resistance of the emitter to B_1 to that of the interbase resistance R_{BB0} as the intrinsic standoff ratio, which can be calculated using:

$$\eta = \frac{R_{B_1}}{R_{B_1} + R_{B_2}} = \frac{R_{B_1}}{R_{BB0}} \tag{2}$$

Figure 3(a) depicts the emitter current vs voltage characteristic curve for a typical UJT.

As the emitter voltage, V_E increases further, the emitter current, I_E increases until the peak point, V_P, beyond which the high level of current injection results in a negative resistance region, as can be seen from figure 3.

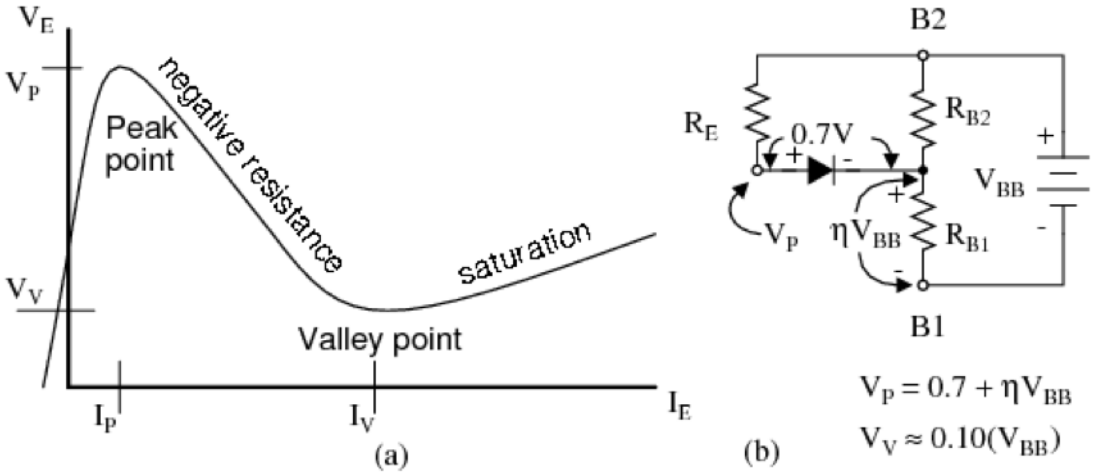

Figure 3: (a) Emitter Characteristic Curve, (b) Model for Vp

The emitter voltage reaches a minimum at the valley point, V_V where the emitter resistance is minimised. By biasing the UJT in the negative resistance region, it is possible to construct a simple electronic oscillator circuit, as shown schematically in figure 4.

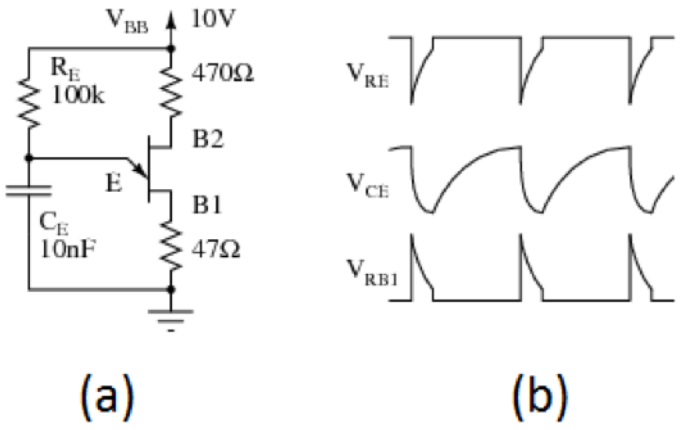

Figure 4: (a) non-linear electronic oscillator circuit using a UJT, (b) Waveforms seen at respective points of the circuit.

The operation of the oscillator circuit shown in figure 4(a) can be described as follows; the external

capacitor, C_E charges based on the current flowing through the resistor, R_E until the voltage at the emitter contact reaches the peak point, V_P. The reduction in the UJT resistance between the emitter and base 1 contacts (due to the negative resistance characteristics) discharges the capacitor. This can be seen in the waveform characteristics in figure 4b. Once the potential across the capacitor has discharged below the valley point, the resistance between the emitter and base 1 increases and the capacitor is free to charge again. This results in a repeating oscillation, where the frequency can be controlled by the selection of the external components. Neglecting any parasitics in the circuit, the oscillation frequency of a UJT oscillator can be expressed as:

$$f = \frac{1}{RC \ln (1/1 - \eta)} \tag{3}$$

To date, no UJT structures have been realised in silicon carbide technology, which precludes this topology from high temperature operation. The requirement for negative resistance in the device operation places significant limits on the carrier lifetime in the semiconductor. At present the typical carrier lifetime in silicon carbide is of the order of 1 μs [14], which is significantly lower than in state of the art silicon or gallium arsenide wafers, where values closer to 1ms are commonplace.

The linear oscillator

In contrast to the non–linear oscillator described in the previous section, the linear or harmonic oscillator produces a sinusoidal waveform. Two fundamental types of linear oscillator are possible; the negative resistance oscillator and the feedback oscillator.

The negative resistance oscillator

The negative resistance oscillator uses an active component that which exhibits negative resistance, such as a magnetron tube, or a diode. Previous research has shown the possibility of Impact ionization avalanche transit-time (IMPATT) diode in silicon carbide, that have suitable characteristics for the realisation of high frequency oscillators [15, 16].

Similar to the non–linear oscillator described in the previous section, the operation of these oscillators relies on the concept of negative resistance. Considering the simple tank circuit shown in figure 5(a), the initial current pulse is applied at I_{in}. The LCR tank responds with a decaying oscillatory behaviour because, in every oscillation a fraction of the energy that reciprocates between the capacitor and inductor is lost as heat in the resistor.

If a device or circuit which exhibits negative resistance is placed in parallel with R_P it can be

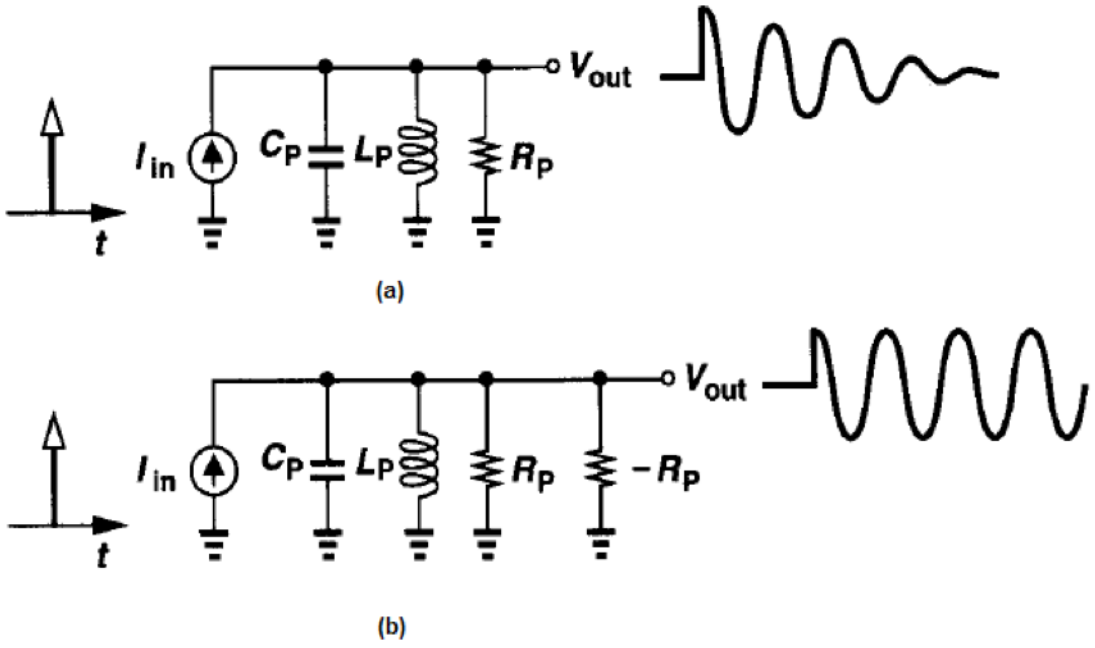

Figure 5: (a) Decaying impulse response of a tank circuit, (b) addition of negative resistance to cancel loss in R_P. [17]

modelled as $-R_P$. If the magnitude of the negative resistance is equal to the parasitic resistance in the tank circuit, R_P, then the circuit continues to oscillate indefinitely, as shown schematically in figure 5b. Such oscillators are used in the production of high frequencies, typically in the microwave region ($>$ 300 MHz) and above. The advantage of silicon carbide in such circuits is its ability to operate at higher temperatures than an equivalent silicon device, thus allowing designers to dissipate much higher levels of power in a circuit [18].

Figure 6a depicts an example oscillator circuit utilising an IMPATT diode as the negative resistance element. The circuit topology in the figure contains a resonant circuit, in this example an LC circuit, but alternatives including those in which a crystal or cavity resonator is connected across a IMPATT diode have identical characteristics.

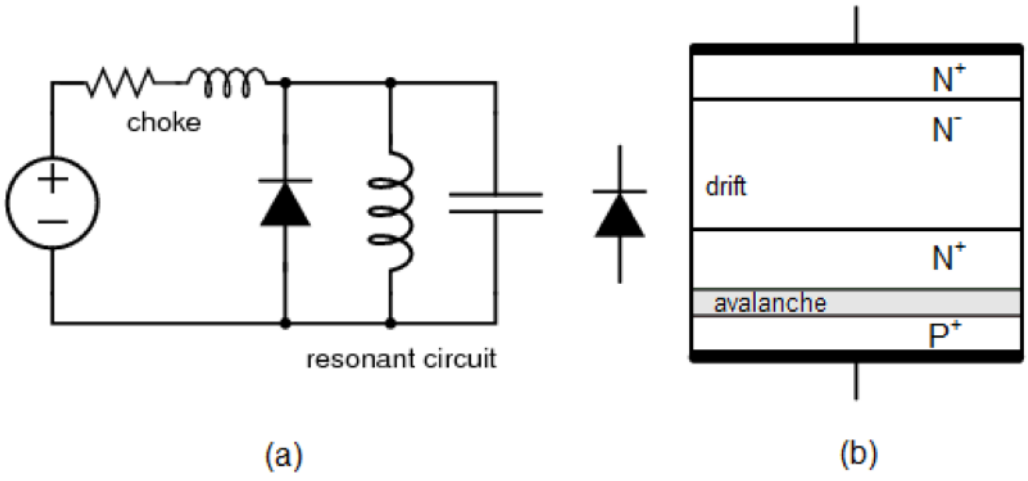

Figure 6: (a) Circuit of a IMPATT diode based negative resistance oscillator (b) Structure of an IMPATT diode

As shown in figure 5a a resonant circuit has the possibility to operate as an oscillator, in that it has the ability to store energy in the form of electrical oscillations if excited. However it will have some form of internal resistance and as a result the magnitude of the oscillations are damped and eventually become zero. The negative resistance of the active device cancels the internal resistance in the resonator, thus creating a resonator where the magnitude of the oscillations shows no evidence of damping. This results in the creation of oscillations with a constant magnitude at the resonant frequency which can be determined using equation 5.

The feedback oscillator

The feedback oscillator is the most common form of linear oscillator. It requires the use of an active component, typically an electronic amplifier based on a single transistor. The output from the amplifier is connected in a feedback loop to the input through a frequency selective electronic filter, resulting in positive feedback. For the oscillator to operate, the gain of the two stages of the amplifier need to fulfil the requirement that the product of the gain for the two individual stages, must exceed unity, i.e. $BA > 1$. This limitation can be considered in terms of the energy required to ensure a constant magnitude of the output waveform. A schematic representation of the feedback oscillator is shown in figure 7

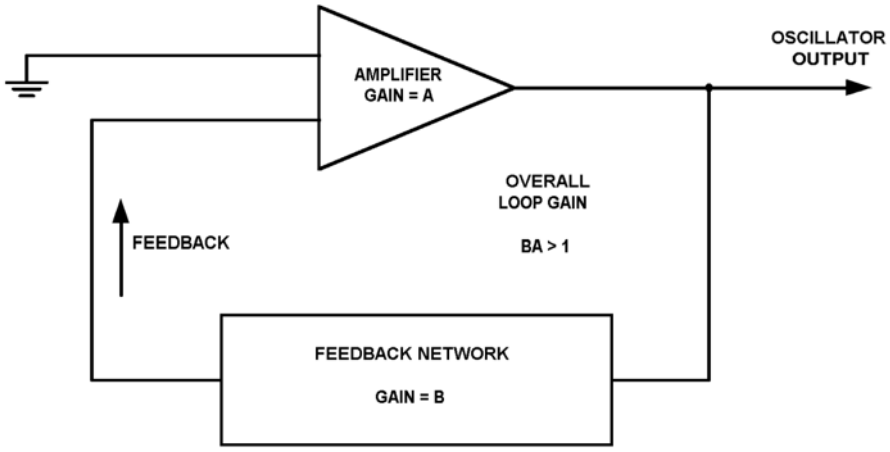

Figure 7: Schematic representation of feedback oscillator

When power is first supplied to the amplifier, the electronic noise in the circuit provides the initial signal to initiate the oscillations. The noise travels around the feedback loop, where it is amplified and filtered until it becomes a sine wave at a single specific frequency.

Feedback oscillator circuits can be classified according to the type of frequency selective filter they employ in the feedback loop. There are three specific types; crystal oscillators, RC oscillators, and LC oscillators each with their own merits and limitations.

Crystal oscillators

Crystal oscillators utilise a piezoelectric crystal as the filter in the feedback loop. The crystal mechanically vibrates as a resonator and the frequency of vibration determines the oscillation frequency of the electronic circuit. A common example circuit for a crystal oscillator is the Pierce oscillator, as shown schematically in figure 8.

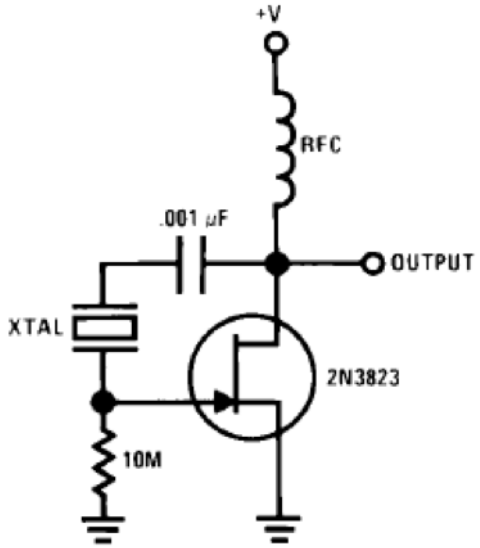

Figure 8: A Pierce crystal oscillator utilising a JFET as active device

Crystals for electronic circuits are typically manufactured from Quartz. Quartz mechanical resonators typically have a very high Q-factor, resulting in a high selectivity to the desired frequency in the feedback loop. In addition, the oscillator frequency showing a weak temperature dependence in comparison to tuned circuits. These two characteristics mean that crystal oscillators have significantly better frequency stability than either LC or RC oscillators. However, quartz is not suitable for the development of high temperature oscillators because it undergoes a phase transition at 573 °C, referred to as the Quartz Inversion [19]. Above this temperature the crystals do not operate as electronic filters and the oscillator produces a wide range of frequencies simultaneously. At the current time, no other material has been identified that can demonstrate the mechanical properties of a quartz resonator and operate at temperatures beyond this temperature. Whilst crystal oscillators provide greater frequency stability with variations in temperature the availability and complexities associated with incorporating a high temperature crystal component were viewed as a disadvantage in comparison the simplicity of prototype high temperature LC Oscillator based circuits. Hence, crystal oscillators have not been experimentally investigated further.

RC oscillators

RC oscillators utilise a filter network comprised of discrete resistors and capacitors to produce lower frequencies (in comparison to the microwave frequencies generated using the negative resistance oscillators described above), typically in the kHz frequency range. A common example circuit topology is the phase shift oscillator, as shown in figure 9.

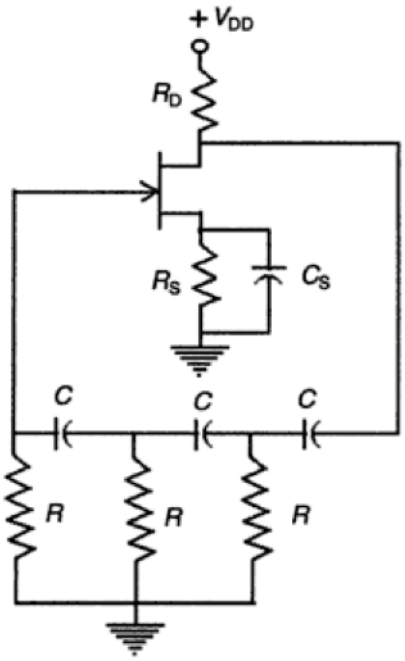

Figure 9: Phase shift oscillator utilising a JFET [24]

It can be seen from the figure that the JFET is operating as an inverting amplifier, producing an output signal which is phase shifted by 180° in comparison to the signal at the input. In this topology, the RC network shown in the lower part of the image acts as a phase shift network. This phase shift in this part of the circuit matches that of the transistor, resulting in a fully in–phase signal. The phase shift is generated by the three RC sections in cascade, each of which produces a 60° phase shift. In general, each of the three sections share common values for the resistance and capacitance of the components. In this case, the frequency of oscillation excluding parasitics can determined from

$$f = \frac{1}{2\pi RC\sqrt{6}} \tag{4}$$

Monolithically integrated RC oscillators (where the resistors and capacitors are fabricated on the same semiconductor die as the JFET) are possible. Because of the limited values of capacitance and resistance that can be realised, these circuits typically operate in the MHz regime, however the gate – source capacitance and channel resistance of the JFET become comparable to the component values, limiting the maximum oscillation frequency.

LC oscillators

In an LC oscillator, the filter is a tuned circuit commonly referred to as a tank circuit, which consists of an inductor and a capacitor connected in parallel. During operation, charge flows back and forth between the plates of the capacitor through the inductor. This transfer of charge occurs at the resonant frequency and so the tank circuit acts as a filter, where the frequency is determined by the capacitance and inductance values. The value is often expressed in terms of the resonant angular frequency, which can be calculated from

$$\omega_0 = \frac{1}{\sqrt{LC}} \tag{5}$$

Where L is the inductance in Henries, and C is the capacitance in Farads

The internal losses within the tank circuit are compensated by the amplifier, which draws energy from the DC supply used in the circuit, resulting in a constant oscillation magnitude. LC oscillators are most commonly used at radio frequencies, where a tuneable frequency source is required. Three commonly used circuit configurations are the Hartley, Colpitts and Clapp oscillators, as shown in Figures 10 a, b and c respectively.

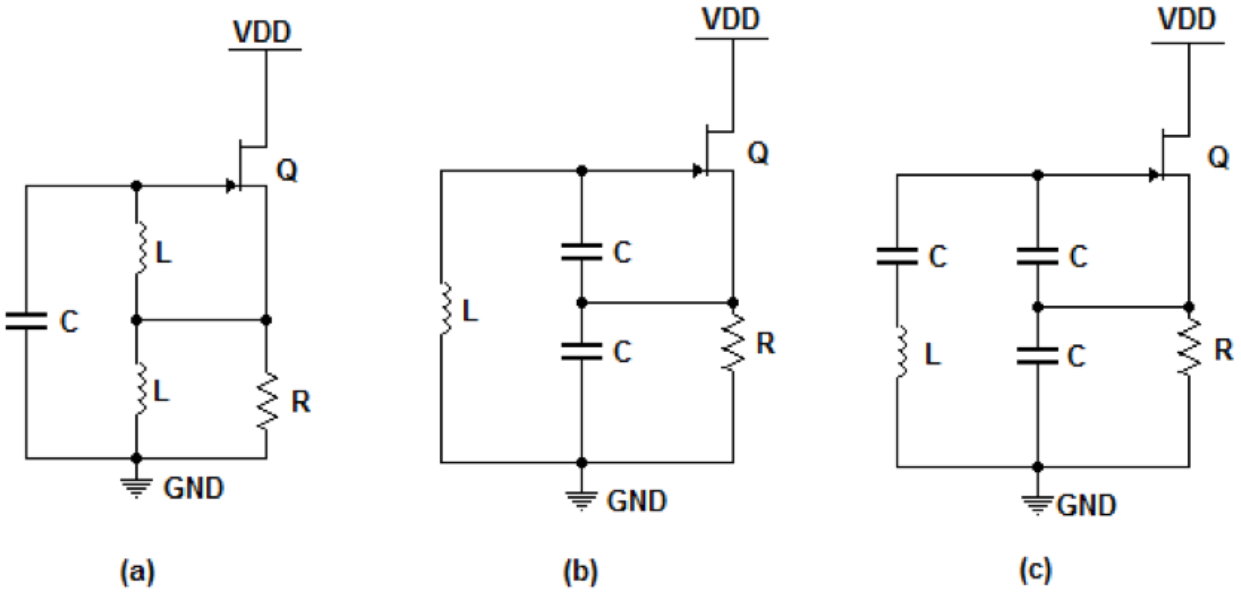

Figure 10: (a) Hartly, (b) Colpitts and (c) Clapp oscillators

As can be seen from the schematic circuits shown in the figure, the Colpitts and Clapp oscillators lend themselves more easily to miniaturisation than the Hartley oscillator circuit, as they only utilise a single inductor in the design. High temperature inductors tend to be physically large, as the permittivity and saturation magnetisation of magnetic materials reduces with increasing temperature [22] and so the Hartley oscillator will be significantly larger than either the Colpitts or Clapp circuits. In this work a Colpitts oscillator design was selected due to the ability of the oscillations to self start

utilising components with lower Q values than the slightly more complicated Clapp design and this offers a more relaxed set of design criteria.

The Colpitts oscillator

The Colpitts oscillator is a common form of LC oscillator which utilises a LC tank circuit and an active device to counter act the damping effect caused by the parasitic resistances. A Colpitts oscillator can be realised using a single transistor acting as amplifier with the addition of a tank circuit. The circuits considered here are based on the use of a depletion mode SiC JFET, however the analysis can be expanded to include a wide range of alternative transistor families, including metal–oxide–semiconductor field effect transistors (MOSFETs) and bipolar junction transistors (BJTs) as well as thermionic valves. By feeding the signal back from the output of the amplifier to the input through this LC tank to select a single frequency, it is possible to commission a Colpitts oscillator circuit, as shown by the circuit given in figure 11.

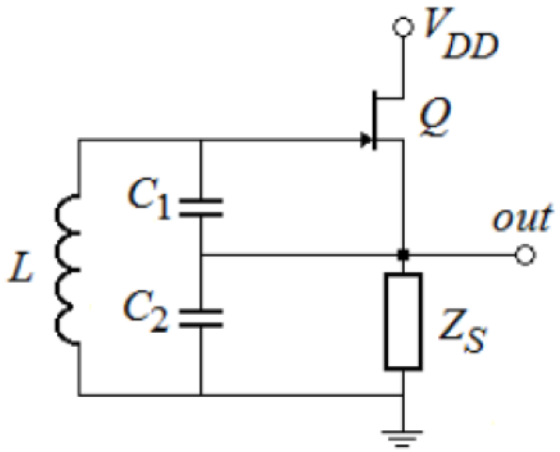

Figure 11: Circuit schematic of a Colpitts Oscillator

The analysis of operation for a Colpitts oscillator is often performed using a linear systems feedback approach, as is described in a number of references, including [22]. The main outcome from this approach is a set of expressions for both frequency and the minimum JFET gain in order for the oscillations to maintain a constant magnitude with time. These conditions are described in equations shown in equations 6 and 7 respectively.

$$f_0 = \frac{1}{2\pi\sqrt{L\frac{C_1C_2}{C_1+C_2}}} \tag{6}$$

$$g_m r_o = \frac{C_2}{C_1} \tag{7}$$

This approach typically results in higher calculated frequencies than those predicted using computer based simulation tools (for example Simulation Program with Integrated Circuit Emphasis – SPICE) or obtained experimentally due to the exclusion of the gate – source, gate – drain and source – drain capacitances within the JFET. It is also possible to use model the characteristics of the Colpitts oscillator using an alternative approach that is based on the concept of negative resistance [9] in one-port oscillators such as the silicon carbide IMPATT diode, replacing the transistor with an ideal entire circuit which has the parasitics explicitly defined as external components, as shown in figure 12

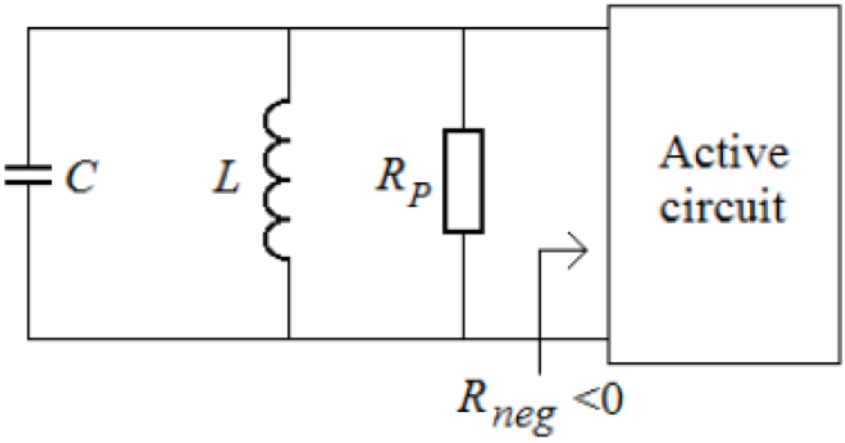

Figure 12: RLC tank with negative resistance created by the Oscillator active network

From the figure it can be see that in order to overcome the energy loss from a finite R_P, the active circuit must form a small-signal negative resistance ($R_P < 0$), which is required to replenish the energy lost in every oscillation. Hence, the negative resistance can be interpreted as a source of energy. In this example R_P denotes the equivalent parallel resistance of the tank and for oscillations to be self-starting it is necessary that $R_P + (-R_P) > 0$. As the oscillation amplitude increases, the amplifier will start to saturate, thus decreasing the gain from the feedback loop, until it reaches unity. This steady–state condition satisfies the Barkhausen criterion [23] and the oscillations continue. Once the circuit is operating in the steady state, the two resistances, R_P and $-R_P$ must be of equal amplitude. This analytical approach allows for the inclusion of the parasitic capacitances that are inherent in the JFET structure, thus yielding a far more accurate calculation of the oscillation frequency of the circuit. Neglecting the effect of the inductor in the circuit, an ac equivalent circuit of figure 12 can be used to determine the input impedance, as shown in figure 13. The input impedance of the circuit can be determined from equation 8

$$|Z_S| \gg \left| \frac{1}{i\omega \left(C_2 + C_{DS} \right)} \right| \tag{8}$$

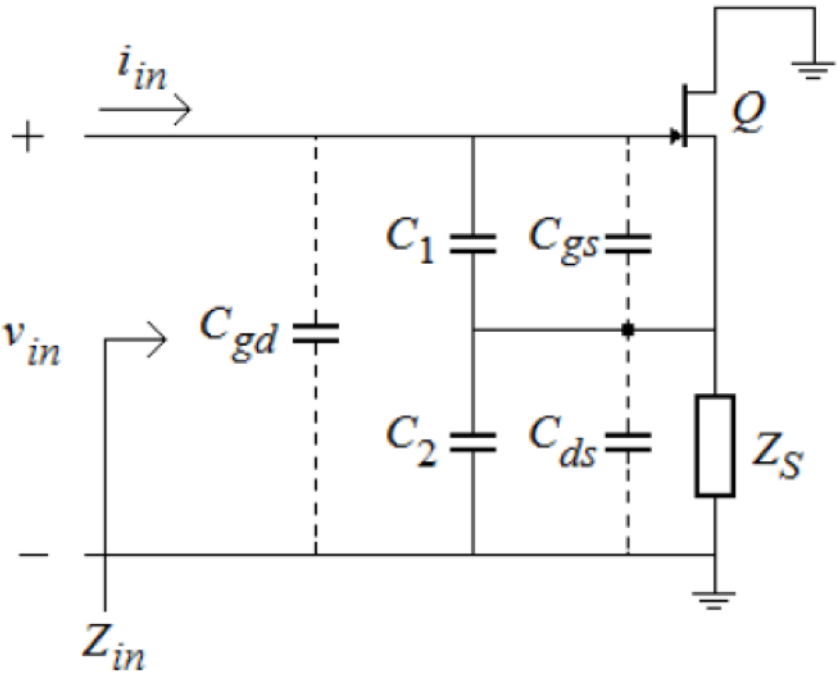

Figure 13: An ac equivalent circuit of a Colpitts oscillator ignoring the inductor L and including the parasitic capacitances inherent in the JFET transistor structure

In figure 13 the parasitic capacitances of the JFET (denoted by Q in the figure) have been included. These are the gate-source, C_{GS} , drain-source, C_{DS} and gate-drain, C_{GD} capacitances. By assuming the following conditions it is possible to describe the JFET by means of a small signal model, which can be utilised within SPICE to accurately describe the behaviour of the circuit.

$$r_{DS} \gg \left| \frac{1}{i\omega \left(C_2 + C_{DS} \right)} \right| \tag{9}$$

$$r_{GS} \gg \left| \frac{1}{i\omega \left(C_1 + C_{GS} \right)} \right| \tag{10}$$

Where r_{DS} and r_{GS} are the small-signal drain-source and gate-source resistances of the JFET . By replacing the SiC JFET, with the simplified small signal model, it is possible to obtain the equivalent circuit of the oscillator shown in figure 14, where is the small-signal transconductance of the SiC JFET.

From results previously published in the literature and utilising standard circuit theory, it is possible to determine the limits for the negative resistance required to achieve steady state operation for the circuit shown in figure 14;

$$r_{neg} = -\frac{g_m}{\left[\omega^2 \left(C_1 + C_{GS} \right) \left(C_2 + C_{DS} \right) \left(1 + \frac{C_{GD}}{C_1 + C_{GS}} + \frac{C_{GD}}{C_2 + C_{DS}} \right) \right]} \tag{11}$$

and the equivalent total capacitance in the circuit C_t can be expressed as

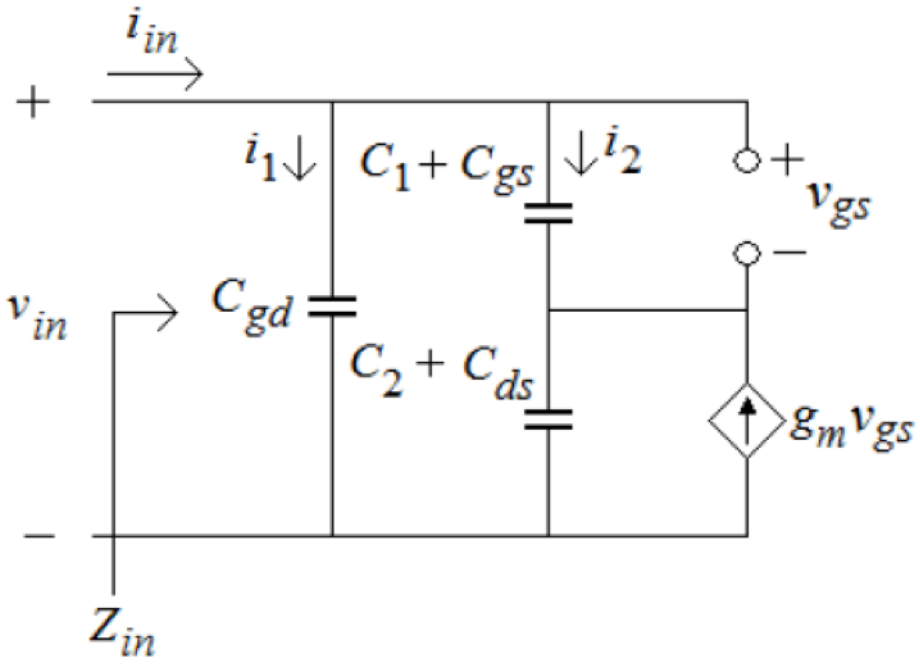

Figure 14: Small-signal equivalent of the Colpitts Oscillator

$$C_t = \frac{(C_1 + C_{GS})(C_2 + C_{DS})}{C_1 + C_2 + C_{GS} + C_{DS}} \left(1 + \frac{C_{GD}}{C_1 + C_{GS}} + \frac{C_{GD}}{C_2 + C_{DS}}\right) \tag{12}$$

It should be noted that combining equation 12 with equation 5 results in the reduction to a well-known expression for the negative resistance [17, 24]:

$$r_{neg} = -\frac{g_m}{\omega^2 C_1 C_2} \tag{13}$$

Utilising these values and reconnecting the inductor, L, along with a series total loss resistance, r_t, to the input impedance, Z_{in}, it is possible to obtain a series equivalent circuit of the Colpitts oscillator, shown schematically in figure 15.

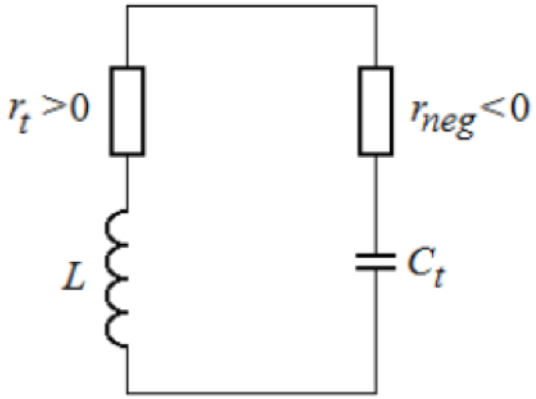

Figure 15: High temperature Colpitts oscillator circuit diagram

Where r_t the total series loss resistance can be calculated from the series resistance of both the

capacitors and inductors using:

$$r_t = r_L + r_{C_1} + r_{C_2} \tag{14}$$

Hence, the equivalent parallel resistance of the Colpitts oscillator, R_P, including contributions from the tank circuit can be determined from

$$R_P = \frac{L}{r_t \frac{(C_1+C_{GS})(C_2+C_{DS})}{C_1+C_2+C_{GS}+C_{DS}} \left(1 + \frac{C_{GD}}{C_1+C_{GS}} + \frac{C_{GD}}{C_2+C_{DS}}\right)} \tag{15}$$

By substituting in equation 12 into equation 5, the oscillation angular frequency for a circuit including the parasitic components can be determined using

$$\omega = \sqrt{\left(L \frac{(C_1 + C_{GS})(C_2 + C_{DS})}{C_1 + C_2 + C_{GS} + C_{DS}} \left(1 + \frac{C_{GD}}{C_1 + C_{GS}} + \frac{C_{GD}}{C_2 + C_{DS}}\right)\right)^{-1}} \tag{16}$$

Substitution of equation 16 in to equation 11 results in

$$r_{neg} = -\frac{g_m L}{C_1 + C_2 + C_{GS} + D_{DS}} \tag{17}$$

Finally referring back to figure 13, it is possible to determine the negative resistance required for the Colpitts oscillator to self–start, resulting in :

$$r_{neg} = -\frac{(C_1 + C_2 + C_{GS} + C_{DS})^2}{g_m (C_1 + C_{GS})(C_2 + C_{DS}) \left(1 + \frac{C_{GD}}{C_1+C_{GS}} + \frac{C_{GD}}{C_2+C_{DS}}\right)} \tag{18}$$

Equation 18 shows that for the circuit to operate, the JFET needs to have a high transconductance, g_m and low parasitic capacitances, C_{GS} and C_{GD}. This identifies the challenge of designing high temperature oscillators, in so much that in addition to the external capacitance values remaining unchanged (the parasitic capacitances within the transistor have a weak temperature dependance), the transconductance of the JFET will limit the upper operating temperature of the circuit. The transconductance of a JFET can be expressed as

$$g_m = \frac{\Delta(I_{DS})}{\Delta(V_{GS})} = \frac{2I_{DSS}}{|V_P|} \left(1 - \frac{V_{GS}}{V_P}\right) \tag{19}$$

High temperature Colpitts oscillator

To demonstrate the importance of an accurate model in determining the resonant frequency of an oscillator, a comparison between the different circuit topologies was performed. Experimentally deter-

mined parameters for silicon carbide devices operating at high temperatures were used in simulations using both SPICE based simulations and the theoretical analysis described in the previous section. The characterised silicon carbide components were then packaged into a hybrid module circuit board which was fabricated on an Aluminium oxide ceramic substrate. Figure 16 shows a schematic representation of the high temperature Colpitts oscillator, with the room temperature component values shown. The hybrid module was placed inside of a Carbolite oven with electronic temperature control during the measurements and allowed to settle for twenty minutes at each temperature prior to any measurements being taken. The frequency spectrum of the oscillator was measured using an Agilent E4403B spectrum analyser, which was coupled to the RF output of the circuit under test.

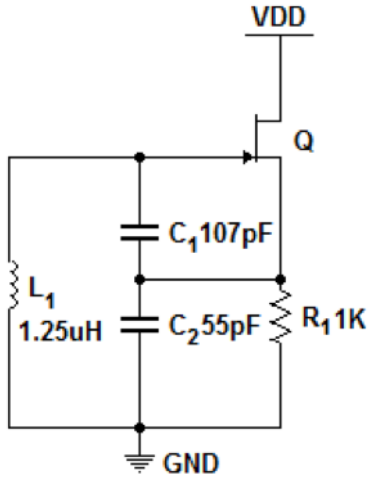

Figure 16: Comparison of calculated, simulated and experimental frequencies as a function of ambient temperature

High temperature voltage controlled oscillator

The data in figure 17 compare the calculated, simulated and experimental frequencies of a high temperature Colpitts oscillator at temperatures up to 573 K. It can be seen from the experimental data that the frequency of the oscillator reduces with increasing temperature. This reduction is due to both the increased capacitance density of the AlN dielectric capacitors, which results from the increasing dielectric constant and the increasing parasitic capacitance of the capacitance of the JFET p–n junction. As can be seen from the data, the predicted oscillator frequency using traditional theory is significantly higher than that obtained experimentally, predominantly because of the parasitic capacitances and inductances in the fabricated circuit. Estimating the parasitic values for the circuit result in modified values, as shown in the figure, however the variation of the modified values with temperature does not match the experimental data well. This indicates that the performance of the oscillator circuit is dominated by the shift in the characteristics of the AlN capacitors. The varia-

tion in the capacitance density of AlN capacitors has been extracted from the capacitance–voltage characteristics [28] and this can be included as a temperature dependence in the SPICE model of the circuit, resulting in the data set labelled as 'Frequency Simulated' in the figure. This shows a better agreement with the experimental data for temperatures above 400 K, however the low temperature frequency is over estimated, similar to the modified theoretical predictions.

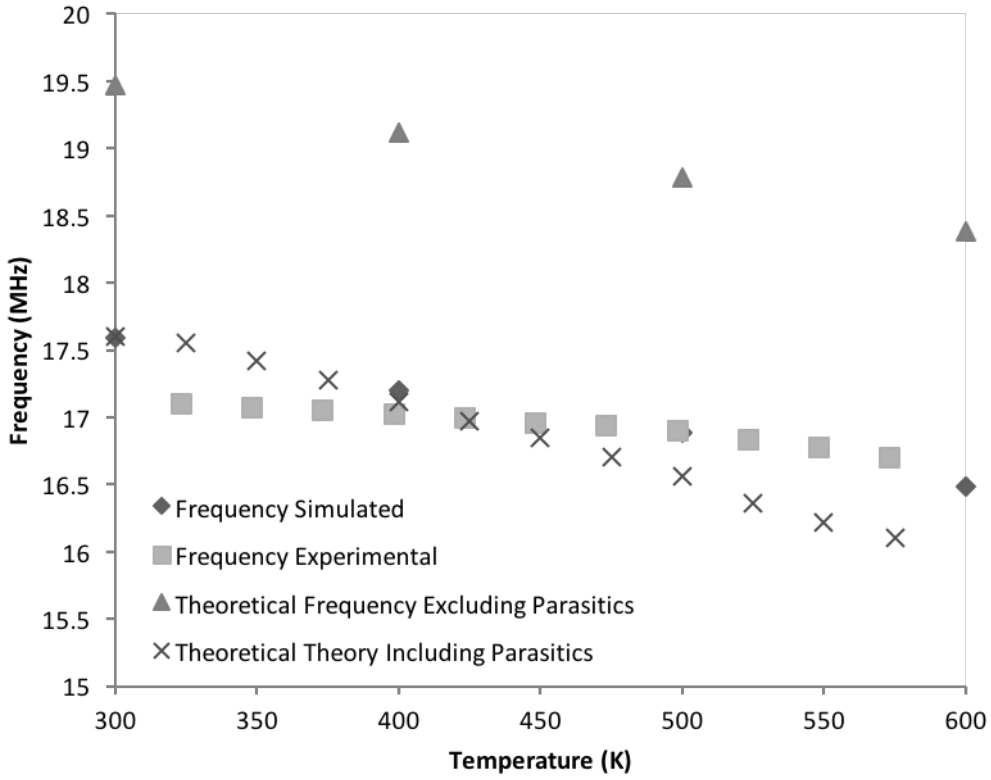

Figure 17: Comparison of calculated, simulated and experimental frequencies of a silicon carbide Colpitts oscillator as a function of temperature

A working communication system requires receiver electronics that are tuned to the specific frequency of the carrier waveform generated by the oscillator circuit. Whilst it is possible to create complicated receiver electronics capable of tracking a drifting signal, the challenge of then demodulating information stored in the carrier signal becomes significantly more difficult. For this reason, it is far more desirable to directly control the frequency of the oscillator in the transmission system. For oscillator circuits based on LC tanks, this is commonly achieved with a device known as a varactor. A varactor is p–n diode that has been optimised to give a significant capacitance under reverse bias conditions, rather than a conventional p–n diode structure where reverse bias capacitance is minimised to increase the switching speed. Since p–n diodes under reverse bias exhibit a depletion region, the width of which varies with voltage, the capacitance of these devices is inversely proportional to the square root of applied voltage. Although a small number of reports of silicon carbide varactors can be found in the literature [26, 27], it is worth noting that all diodes, including silicon carbide Schottky diodes exhibit an identical change in capacitance with applied bias. For this reason, it is possible to

modify the high temperature Colpitts oscillator circuit shown in figure 15 to form a high temperature voltage controlled oscillator by the inclusion of a Schottky diode, resulting in the circuit shown in figure 19.

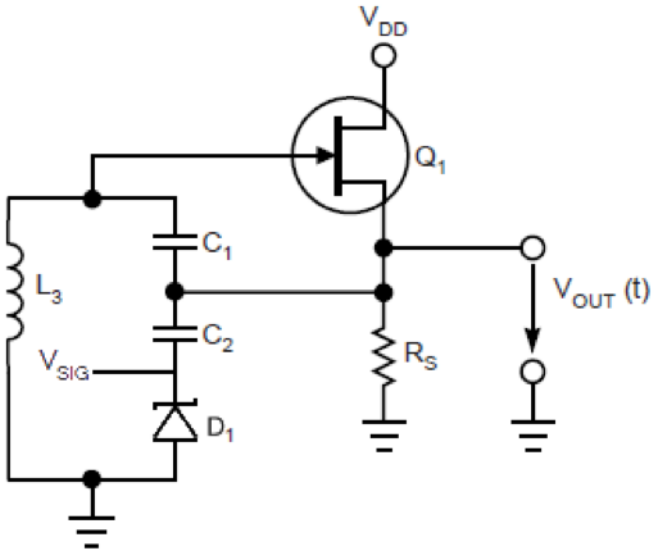

Figure 18: Circuit schematic of a high temperature voltage controlled oscillator

Neglecting the effects of the JFET junction capacitance and any stray capacitance from the circuit on the frequency of the oscillations, the addition of a reverse biased silicon carbide Schottky diode acting as a varactor can be considered as adding two capacitors, denoted by C_2 and D_1, in series as part of the tank circuit. This results in a capacitance that is voltage dependent in the lower branch of the tank circuit and the oscillator frequency (ignoring the influence of parasitics in the circuit) can now be approximated by

$$f = \frac{1}{2\pi\left(\sqrt{L\frac{C_1 C_{TOT}}{C_1 + C_{TOT}}}\right)} \tag{20}$$

where C_{TOT} is the capacitance of the Schottky diode and C_2 in series

The capacitance of the Schottky diode can be decreased by the application of an external bias to the V_{SIG} port shown in figure fig18 and can be expressed as.

$$C = A\left(\frac{q\epsilon}{2}\right)^{0.5}\left(\frac{N_D}{\phi_B - V_A}\right)^{0.5} \tag{21}$$

where A is the diode area, ϵ the dielectric constant of the silicon carbide, q the electronic charge, N_D the dopant concentration in the n–type region (assuming the abrupt junction approximation), ϕ_B the barrier height, V_A the applied bias.

The data in figure 19 show the variation in the capacitance of a silicon carbide Schottky diode as a function of reverse bias for the range of temperatures of interest. The observed decrease in

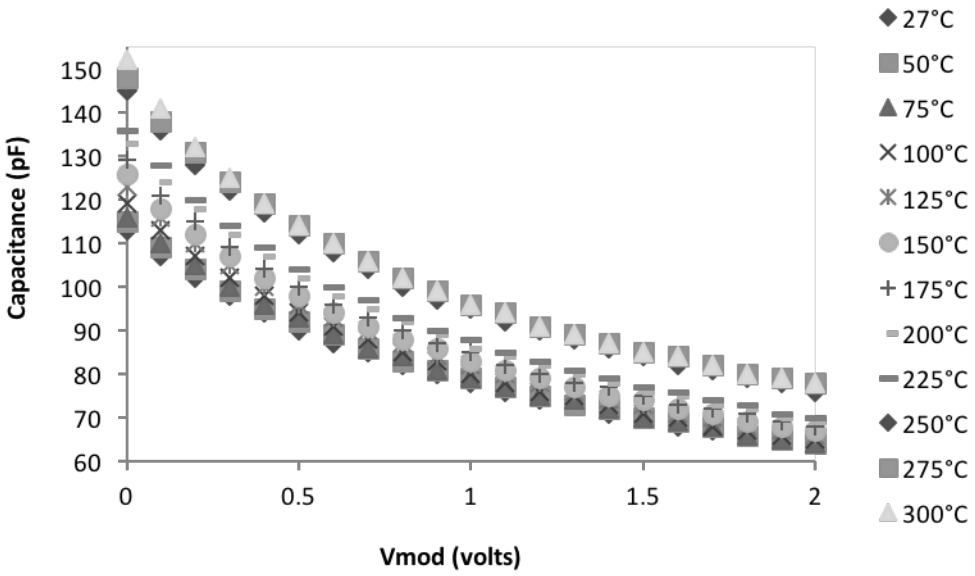

Figure 19: Capacitance of a SiC Schottky diode with different applied voltage bias as a function of temperature

capacitance with increasing temperature is linked to the increasing depletion width formed in the of the device, which results in the decreasing capacitance of the diode, as is expected from parallel plate capacitor theory [14]. Note that the capacitance of D_1 is in series with the capacitance of C_1 and so it is possible to control C_{TOT} by applying a voltage to D_1. This results in the decrease of C_{TOT} and hence an increase in the resonant frequency of the oscillator, as described by equation 20 and can be seen from the data plotted in figure 20.

As shown by the data in figure 20 it is possible control the frequency of a silicon carbide SiC Colpitts based voltage controlled oscillator across a wide temperature range. The data show the potential to create an electronic feedback loop to stabilise the resonant frequency of the circuit through the application of a bias at the V_{SIG} port of the circuit. This technique can be used to nullify the temperature dependence of the oscillator for temperatures between 273 and 573 K. This technique can also be used to achieve direct frequency modulation of the oscillations and hence open up the possibility of generating modulated signals that can be utilised for data transmission in extreme environments.

Modulation

Modulation is the term used to describe the process of varying one or more properties of a periodic waveform. The high frequency carrier signal is modulated with a lower frequency signal (often referred to as the secondary signal) which typically contains the information to be transmitted [12]. In principle three basic methods of modulating the carrier waveform are practical and they can be implemented

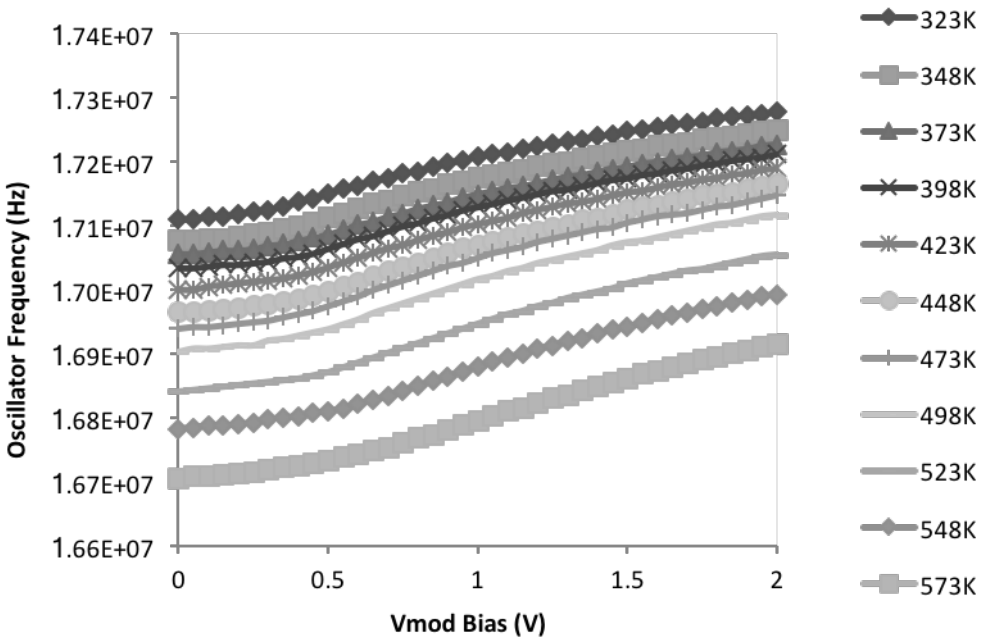

Figure 20: Frequency range of SiC Voltage Controlled Oscillator

using either analogue or digital methods. Figures 21 a, b and c show schematically examples of Amplitude Modulation (AM), Frequency Modulation (FM), and Phase Modulation (PM) schemes respectively.

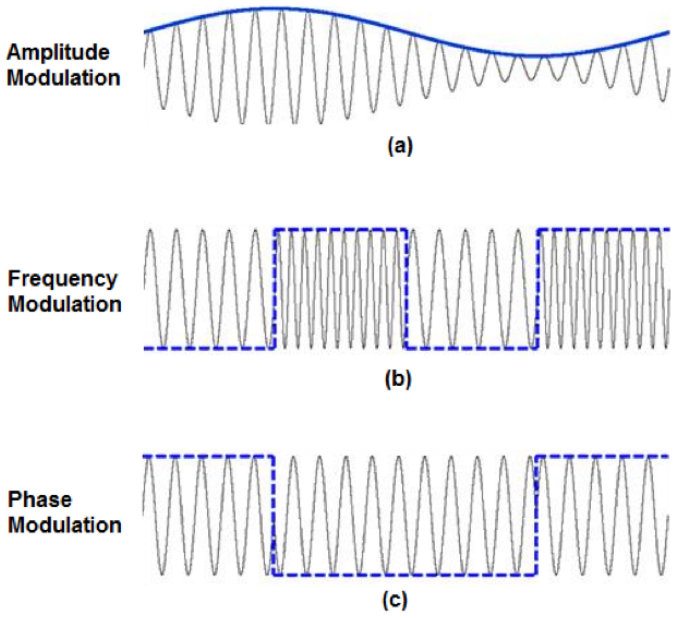

Figure 21: Example Waveforms showing a) Amplitude Modulation, (b) Frequency Modulation, (c) Phase Modulation

Considering the amplitude modulation (AM) scheme, shown in figure 21, the carrier waveform of a set frequency is combined with an analogue information signal by modulating the amplitude of the carrier signal. This is one of the simplest forms of communication system, however data fidelity can be compromised by temporary changes in the efficiency of the communications channel between the transmitter and receiver, such as changes in weather or passing people. It is possible

to utilise this method in an engineering context for the transmission of low data rate, non critical digital signals for short distances, however in order to achieve the performance required for a wireless sensor node alternative modulation schemes are required. Figure 21 b is an example of a frequency modulation (FM) scheme implemented using digital techniques, where the amplitude of the carrier waveform remains constant, whilst the frequency is varied between two distinct states. Each of these two states is used to represent a binary number. Whilst this modulation system has a greater level of complexity for both the transmitter and the receiver, the significant increase in data fidelity has made this modulation scheme extremely popular for the transmission of data from wireless nodes. An example of a digital Phase Modulation scheme is depicted in figure 21 c. In this scheme, the magnitude and frequency of the signal remains constant, whilst the phase of the waveform is shifted by 180° to indicate the different binary numbers. This scheme offers the potential of the greatest information density, but with the highest level of complexity – often using microprocessors to control the transmitter and receiver in real time.

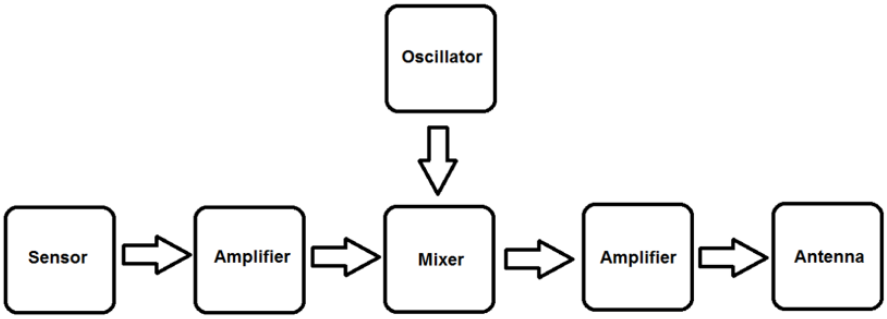

Figure 22: Block diagram of a simple analogue AM communications system

Figure 22 shows a schematic representation of a simple analogue AM communications system that is suitable for implementation in silicon carbide technology. In this example, the analogue signal used to modulate the carrier waveform could be produced using a sensor either directly or through previous amplification electronics. The amplitude of the modulation signal is directly proportional to the signal on the sensor and so AM modulation can be achieved by means of a mixer circuit. The mixer ensures that the output amplitude of the oscillator is modulated by the magnitude of the sensor signal. This is the basis of a creates a simple analog communications system where the amplitude of the carrier signal can be directly related to the sensor. The amplifier needs to demonstrate a high linearity at a single frequency to ensure that the data fidelity is maintained and to avoid complex deconvolution at the receiver.

Previously in this chapter it has been shown that by utilising SPICE models for the SiC JFET and Schottky diode along with the characteristics of the high temperature passive components, it is

possible to design, simulate and commission a high temperature Colpitts oscillator using SiC devices. Here this is extended to show that the amplitude of the carrier signal can be directly modulated at 280C [10]. Using the schematic circuit shown in figure 15 as the Colpitts oscillator, capacitors fabricated from AlN dielectric C_1 and C_2 were selected to have values of 68 pF and 82 pF respectively. The choice of AlN as the dielectric was to minimise the leakage current through the capacitors and to enable the integration of the capacitors with the dielectric films commonly used in the fabrication of high temperature packages. A high temperature printed circuit board was commissioned from a thick gold film on a ceramic substrate. The approximate frequency of the LC Tank was determined from the physical size of the inductor, L. Based on equations 20 and 22 the frequency of the oscillations was predicted to be approximately 22 MHz for an inductor value of 1.4 μH. The load resistor in the circuit was set to 1 kΩ, and 12 V DC was supplied to the circuit at the drain of the JFET denoted by Q. The inductance of a planar spiral can be determined from

$$L = \frac{N^2 \left(\frac{D_i + N(W+S)}{2}\right)}{30 \left(\frac{D_i + N(W+S)}{2}\right) - 11 D_i} \tag{22}$$

where N is the number of turns on the inductor, D_i the diameter of the innermost turn, N the number of turns, W the width of the tracks and S the spacing between the turns.

Simulations of the oscillator circuit based on the experimental device parameters extracted indicate that the oscillator is capable of self starting, as shown by the data in figure 23.

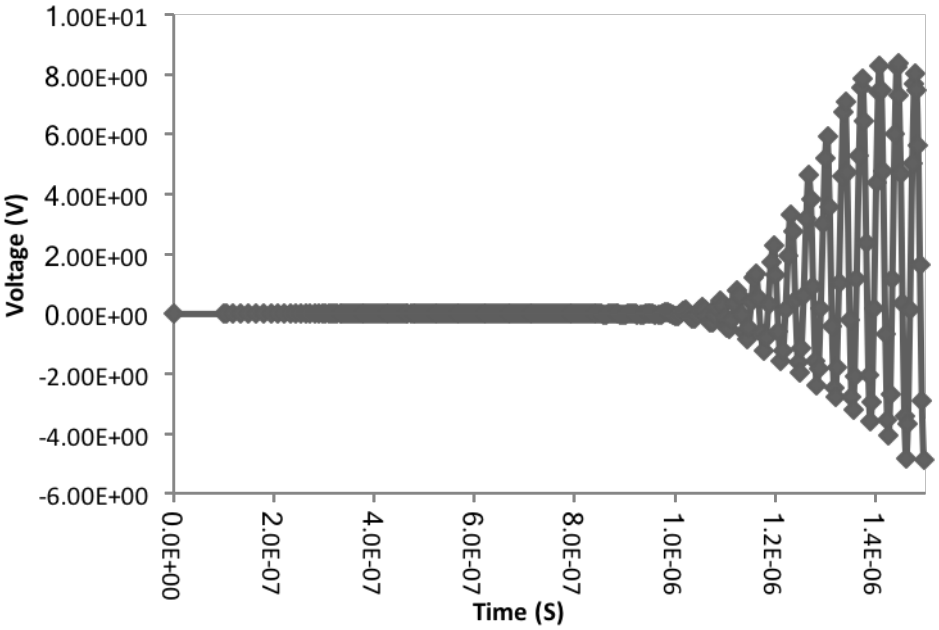

Figure 23: Spice simulation of the self starting of a Colpitts oscillator

This indicates that the transconductance of the SiC JFETs used in the circuit is sufficient to ensure that the Barkhausen criteria is met and the oscillations continue indefinitely. By modifying

the Colpitts oscillator circuit to that shown by the schematic in figure 24, it is possible to utilise a second active component to produce amplitude modulation of the carrier waveform.

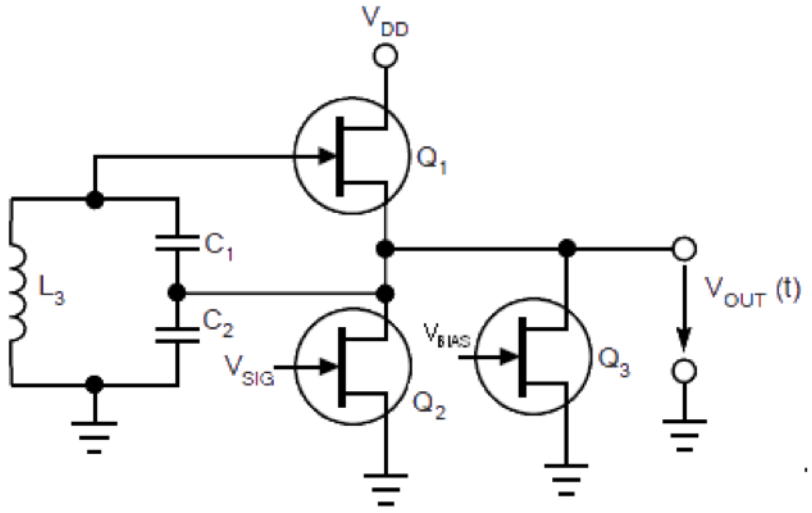

Figure 24: Circuit schematic used in high temperature modulation experiment

The amplitude of the oscillations are varied by changes in the amplitude of the feedback signal seen at the gate of JFET denoted by Q_1. This is achieved by utilising JFET Q_2 as a variable resistor. A negative bias on the gate of Q_2 (in respect to the source of the JFET) which is designated as V_{SIG} in the figure, it is possible to control the resistance of the JFET channel and therefore the magnitude of the feedback signal to the gate of Q_1. This can be clearly observed in the data shown in figure 24, where a 1 MHz sinusoidal signal was fed into V_{SIG}. This resulted in changes to the channel resistance of JFET Q_2 and this directly modulates the feedback seen at the capacitance tap. The effect of this change in the capacitance feedback can be observed by increasing the negative bias on V_{SIG}, which results in the amplitude of the carrier signal increasing. This can ultimately be used to create an amplitude modulated signal at the JFET gate, which is also the signal transmitted through the inductor.

A hybrid module was then assembled using a 1000 μm thick aluminium nitride substrate, onto which a seed layer of 10 nm chrome was deposited by physical vapour deposition followed by 250 nm of gold. The gold layer on the substrate was then electroplated to a thickness of approximately 8 μm, to reduce the track resistance. Capacitors fabricated with a60 nm thick HfO_2 dielectric, selected for low leakage characteristics (sub μA at 5 V) with values of 68 pF (C_1) and 82 pF (C_2) respectively. The inductor, denoted by L_3 was a gold spiral patterned directly onto the substrate. The frequency characteristics of the inductor were determined at 1 MHz using an Agilent 4284A LCR bridge which demonstrated an inductance of 1.4 μH and a resistance of 4.8 Ω. The capacitors and JFETs were then attached to the circuit using silver epoxy, which was baked at 150 °C for 1 hour, prior to the electrical connections being made by gold wire bonding. The frequency spectrum of the oscillator

was measured using an Anritsu MS2721B Spectrum Master and the amplitude of the RF signal was measured through an external aerial attached to a Tektronix TDS3045C oscilloscope.

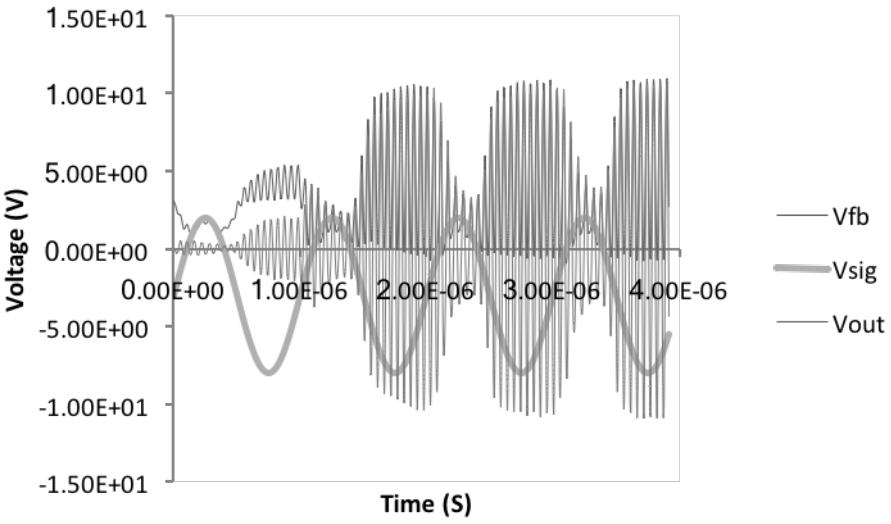

Figure 25: Simulated output characteristics of the circuit shown in figure 24

With the gate to Q_3 held at -8V, the application of a modulation signal to the gate of JFET Q_2 varied the amplitude of the output signal as can be observed from the data in figure 25. For an applied bias between -4 V and -6 V (denoted by region B in the figure), increasing the magnitude of V_{SIG}, increases the resistance of the JFET channel.

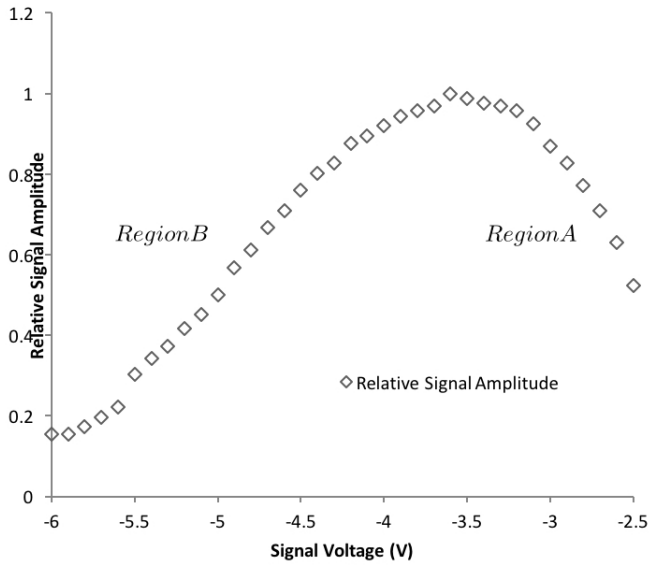

Figure 26: Relative Amplitude of output signal with varying V Bias

As previously described this increases the magnitude of the output signal, with a behaviour that is reasonably linear. For bias levels with a magnitude below 2.5 V the resistance of the channel reduces

the current flowing through the circuit, resulting in a reduction in the amplitude of the oscillations – as can be observed in the region denoted by A in the figure. The data indicate that it is possible to achieve amplitude modulation by varying the voltage applied to Q_2 in two regions. However in region B (the higher bias region) the frequency of the oscillations was observed to vary with the applied bias.

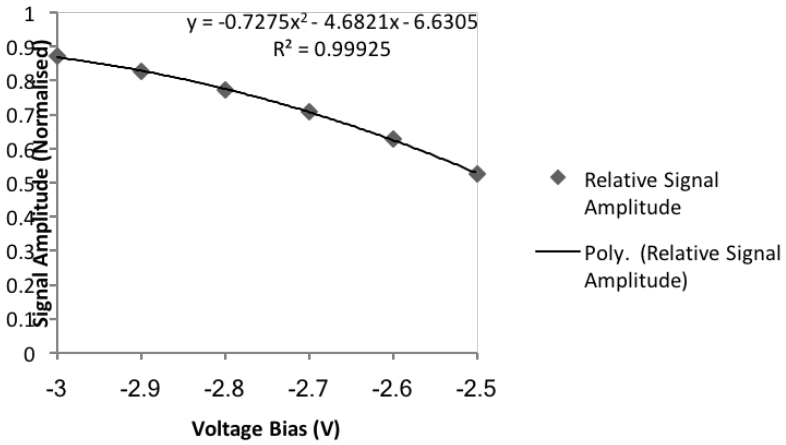

Figure 27: Signal amplitude Vs Voltage bias of region A

This is a non–desired results from a systems perspective as it will require a high level of sophistication in the receiver circuit and so the performance of the circuit operating in region A was investigated further. As shown by the data in figure 27 the variation of the amplitude with the applied voltage is not linear. This originates in the physics behind the operation of the JFET, where the channel characteristics vary with the square of the applied voltage.

The frequency spectrum of the oscillator whilst operating at 280 °C is shown by the data in figure 28. The gate of Q_2 was held at a constant -3.5 V, resulting in the maximum oscillator amplitude. During the measurements, the amplitude of the peak frequency was 65 dBm above the background noise, with a full half width maximum of approximately 7.2 kHz.

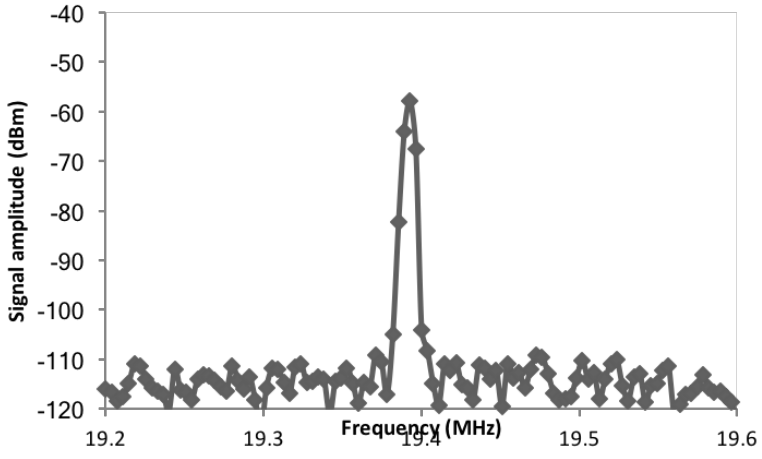

Figure 28: Frequency Spectrum of AM Colpitts Oscillator at 280 °C

The oscillation frequency was measured as a function of temperature to determine the temperature

coefficient of the peak frequency. As can be seen from the data in figure 29, the frequency decreases with increasing temperature, linked to the increased capacitance of the HfO_2 MIM capacitors [28, 29].

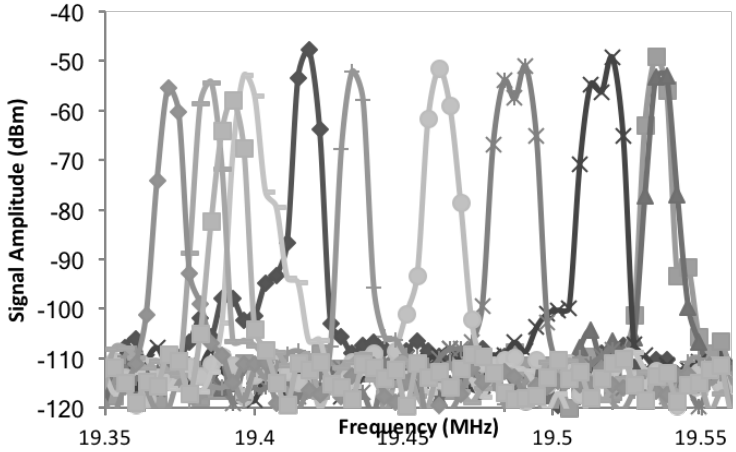

Figure 29: Change in frequency with increasing temperature

The data in figure 30 show that in addition to the frequency shift with temperature, the amplitude of the oscillations also decrease. The data point for 353 K is influenced by a lack of temperature stability in the oven used for the testing, related to the PID parameters being unoptimised for low temperatures. The data for the decrease in signal amplitude with temperature was taken with Q_2 biased at a gate – source potential of -3.5 V to obtain maximum oscillation amplitude and hence maximise the transmitted power. For a high temperature communications system based on Amplitude Modulation to be effective, a feedback system that can maintain the signal amplitude with varying temperatures is essential. With the current maturity level of silicon carbide technology this is not possible, effectively ruling out the possibility of high fidelity data transmission using an amplitude modulation communications link.

Extreme environments are not just classified in terms of the high ambient temperature, high radiation dose rate and the existence of chemically corrosive species, they often include high intensity

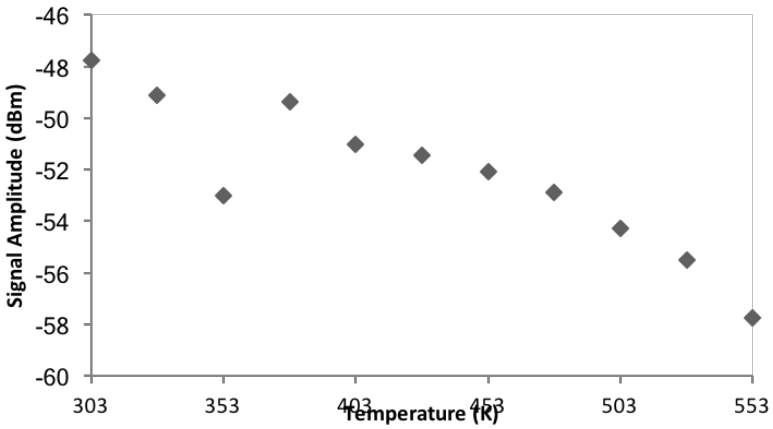

Figure 30: Maximum signal amplitude as a function of temperature

sources of radio frequency interference or noise. Frequency Modulation communication schemes are inherently more resilient to these sources of noise than amplitude modulation schemes [30].

Figure 31shows a schematic representation of a simple frequency modulated communication system, that can be implemented in silicon carbide technology.

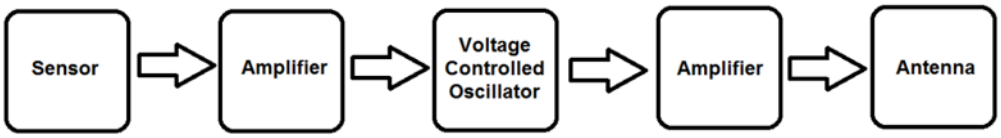

Figure 31: Block diagram of simple FM Transmitter

By replacing the Oscillator and Mixer blocks in the schematic circuit diagram shown in figure 21 with a voltage controlled oscillator circuit, direct frequency modulation of the oscillations can be achieved [30]. In a simple sensor system the sensor output is applied directly to the Varactor diode, varying the depletion capacitance and hence the frequency of a voltage controlled oscillator. This frequency modulated signal is then amplified to an antenna, resulting in an analogue frequency modulated communications system.

However the system is also capable of transmitting data in digital form, as shown by the schematic in figure 20 b. The digital transmission of data by means of frequency modulation of the carrier wave is called frequency shift keying (FSK), in contrast to the amplitude modulated transfer of digital data which is referred to as amplitude shift keying (ASK). Frequency shift keying can be achieved by choosing and transmitting two distinct frequencies to represent the '1' and '0' binary bits. Similarly amplitude shift keying can be achieved by selecting two distinct amplitudes at the same frequency to represent digital information.

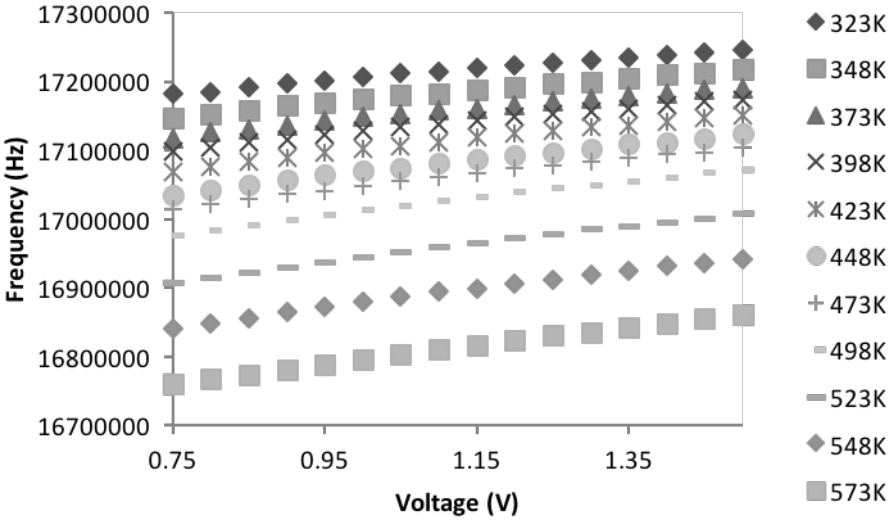

Figure 32: Linear regions of oscillator frequency change

The frequency modulation circuit shown in figure 17 was demonstrated experimentally and assessed at high temperatures, with a view to assessing the possibility of frequency shift keying communications in extreme environments. A hybrid frequency modulation circuit, fabricated using the same techniques as the amplitude modulation circuit described above was tested at temperatures up to 300 °C. As shown by the data in figure 32 the frequency of the oscillator varies linearly with the increasing magnitude of the reverse bias applied (between -0.75 and -1.5 V) to the Schottky diode (D_1). The shift in oscillator frequency for an applied bias of -0.75 and -1.5 V does not show a significant variation with temperature, which indicates that frequency modulation is a suitable technique for dat transmission across a wide temperature range. The observed drift in the oscillator frequency with temperature is caused by the shift in the capacitances in the circuit, as described for the amplitude modulation circuit.

The data in figure 33 shows the only reported frequency shift keyed behaviour from an all silicon carbide circuit which was operating at 300 °C, captured using an Anritsu MS21721B Spectrum Master. The data clearly show two distinct peaks, one located at a frequency of 20 kHz with respect to that of the carrier waveform that represents a digital '1' and the carrier waveform itself, that represents a digital '0'. The peaks are formed by the application of a square wave of 1 kHz to the diode in the voltage controlled oscillator circuit, shown in figure 19. Hence, it is possible to transmit frequency shift keyed data using a silicon carbide oscillator over a range of temperatures that are beyond the capability of conventional, silicon based electronic systems.

Of the different available modulation schemes, frequency shift keying systems are the most power efficient. This is critical consideration for a wireless sensor node, that may be powered by energy harvested from the ambient environment. The disadvantage of this modulation scheme is the low bandwidth efficiency, as they require significant bandwidth for each sensor to operate in a unique frequency range [31] . However there is a special case of frequency shift keyed modulation which addresses this issue and can also be viewed as an attractive alternative to the phase shift keyed modulation which commonly prevails in digital communication systems, such as mobile telephones, due to the higher data rates possible. Minimum shift keying has been has shown to be a special case of continuous phase frequency shift keying, where the frequency deviation equal to the bit rate. Minimum Shift Keying can also be viewed as a form of offset Quadrature Phase Shift Keying signalling in which the symbol pulse is a half-cycle sinusoid rather than the usual rectangular form. This method has the potential to combine in a single modulation format a number of attractive attributes, including constant envelope, compact spectrum, the error rate performance BPSK, and simple demodulation and synchronization circuits. These features make MSK an excellent modulation technique for digital

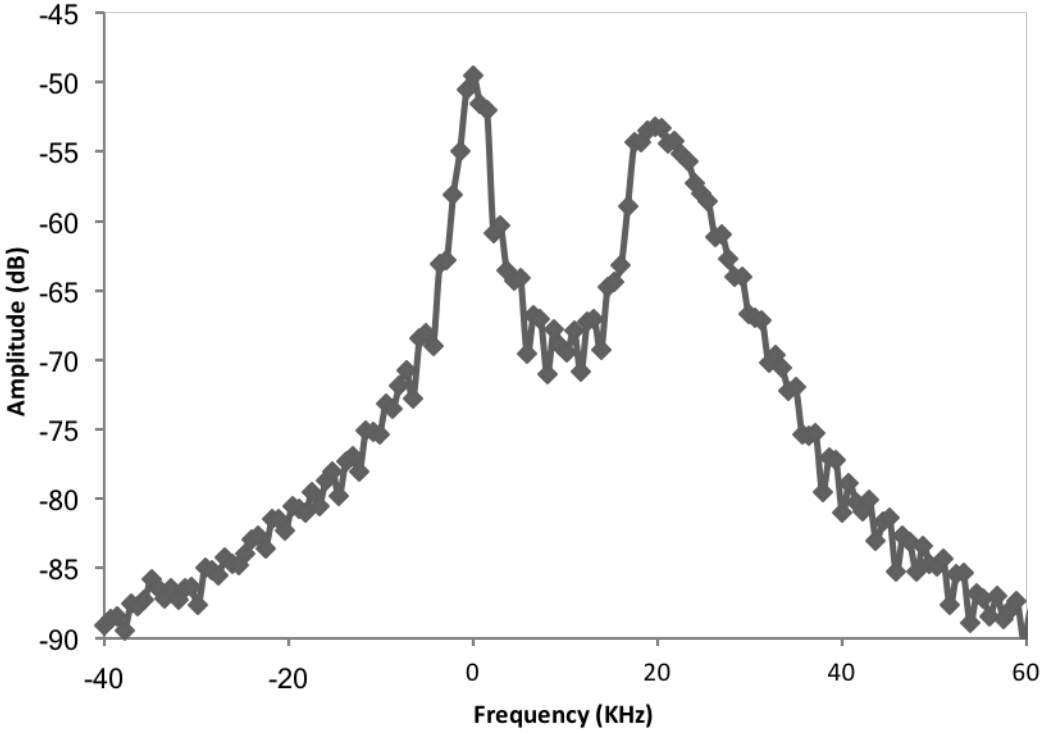

Figure 33: Spectrum showing Frequency shift keyed Modulation

links in which bandwidth conservation and the use of efficient transmitters with nonlinear (amplitude saturated) devices are important design criteria [31]. However, at this stage of the technology maturity, the requirements for this technique cannot be met by silicon carbide devices and so this must remain an option for future developments.

Conclusions

This chapter has demonstrated the possibility of fabricating high temperature electronic oscillators using silicon carbide technology. The low maturity of silicon carbide in comparison to silicon precludes the use of microprocessor controlled oscillators, however analog circuits based on discrete components have been shown to offer performance that is suitable for a wide range of applications. Predictions as to the frequency of the oscillations requires accurate knowledge of the parasitic capacitances in the circuit, but more crucially the variation with temperature of these parasitics and the discrete components used in the circuit. Utilising device characteristics that were determined over the temperature range of interest, a high temperature Colpitts based voltage controlled oscillator was demonstrated. The circuit was used to show that it is possible to control the frequency drift at high temperature along with amplitude modulation and frequency modulation of two high temperature oscillators working

at temperatures up to 300 °C. The physical design of the Colpitts oscillator specifically lends itself to miniaturisation, featuring a capacitive feed-back path, offering greater frequency stability and physically smaller components than the inductive feed-back path found in the Hartley oscillator The Colpitts oscillator also demonstrates an inherently more powerful self starting-up ability than the Clapp oscillator which results in the allowed utilisation of lower components with larger tolerances, which is typical in the low technological maturity silicon carbide devices.. LC oscillators provide a simple solution for producing high frequency sine waves, these circuits contain a tuned LC tank and an active device arranged in an amplifier layout, they are particularity useful in situations where the energy supply can be intermittent due to their self starting ability.

References

1. N.G. Wright, A.B. Horsfall, Journal of Physics D, vol. 40 (2007) pp.6345

2. www.littelfuse.com/products/power-semiconductors/silicon-carbide.aspx

3. www.wolfspeed.com

4. H.K. Chan, N.G. Wood, K.V. Vassilevski, N.G. Wright, A. Peters, A.B. Horsfall, Proceedings of IEEE Sensors conference, 2015

5. M.H. Weng, R. Mahapatra, N.G. Wright, A.B. Horsfall, IEEE Sensors Journal, vol. 7 (2007) pp. 1395

6. J.A. Cooper, M.R. Melloch, R. Singh, A. Agarwal, J.W. Palmour, IEEE Trans. Elect. Dev., vol. 49 (2002) pp. 658

7. C.M. Zetterling, in '*Process Technology for Silicon Carbide devices*', Inspec Publishing, 2002, ISBN 0852969988

8. M.H. Weng, *et al*, Semiconductor Science and Technology, vol. 32 (2017) 054003

9. O. Mostaghimi, N.G. Wright, A.B. Horsfall, Proceedings of ECCE conference 2012, pp. 3956

10. D.R. Brennan, B. Miao, K.V. Vassilevski, N.G. Wright, A.B. Horsfall, Materials Science Forum, vols. 653–956 (2010) pp. 953

11. V. Blahm, T.P. Sylvan, Solid State Design, vol. 5 (1964) pp. 26

12. A.A. Andronov, A.A. VItt, S.E. Khaikin '*Theory of Oscillators*' Dover Publications, (2009), ISBN 0486655083

13. T. Kimoto, K. Yamada, H. Niva, J. Suda, Energies, vol. 9 (2017) pp. 918

14. G. Sozzi, M. Puzzanghera, G. Chiorboli, R. Nipoti, IEEE Trans. Elect. Dev., Vol. 64 (2017) pp. 2572

15. J. Jensen, IRE Trans Circuit Theory, vol. 4 (1957) pp. 276

16. I.M. Gottleib, '*Practical oscillator handbook*' Newnew (1997), ISBN0750631020

17. L.S. Senhouse, IEEE Trans. Elect. Dev., vol. 16 (1969) pp.

18. K.V. Vassilevski, IJHSES, vol. 15 (2005) pp. 899

19. K.V. Vassilevski, IEEE Elect. Dev. Lett., vol. 37 (2001) pp.

20. B. Razavi, in '*Design of analog CMOS integrated circuits*', McGraw Hill, Boston (2016) ISBN 0072524932

21. A.H. Morrish, '*The physical principles of magnetism*', Wiley, New York, (2001), ISBN 9780780360297

22. R. Trew, Proceedings of the IEEE, vol. 79 (1991) pp.

23. D. Leenarts, J. van der Tang, C. Vacher, '*Circuit design for RF transceivers*', Kluwer, Boston (2001), ISBN 9780306479786

24. K. Sanitram, in '*Basic electronics: devices, circuits and fundamentals*' Dover Publications, (1972), ISBN 0486210766

25. S. Barker, B, Miao, D.R. Brennan, N.G. Wright, A.B. Horsfall, Proceedings of IEEE Sensors conference, 2009, pp. 777

26. M. Christer, M. Anderson, IEEE Trans. Elect. Dev., vol. 32 (2011) pp.ńewline 27. N.G. Wright A.P. Knights, A.G. O'Neill, C.M Johnson, Proceedings of EDMO conference 1999, pp. 301

28. B. Miao, R. Mahapatra, N.G. Wright, A.B. Horsfall, Journal of Applied Physics, vol. 104 (2008) 054510

29. B. Miao, R. Mahapatra, R. Jenkins, J. Silvie, N.G. Wright, A.B. Horsfall, IEEE Trans. Nuc. Sci., vol. 56 (2009) pp. 2916

30. D.R. Brennan, K.V. Vassilevski, N.G. Wright, A.B. Horsfall, Materials Science Forum, vol. 717 (2012) pp. 1269

31. R. deBuda, IEEE Transactions on Communications, vol. 7 (1972) pp.